CrystEngComm

Accepted Manuscript

ROYAL SOCIETY OF CHEMISTRY

www.rsc.org/crystengcomm

ARTICLE TYPE www. rsc.org/xxxxxx | XXXXXXXX

Illuminating Protein Crystal Growth using Fluorophore-Labelled Proteins †

Alaa Adawy,*[a‡] Willem J. P. van Enckevort,[a] Elisabeth S. Pierson,[b] Willem J. de Grip[c] and Elias Vlieg [a]

Received Xth XXXXXXXXXX 20XX, Accepted Xth XXXXXXXXX 20XX
First published on the web Xth XXXXXXXXXX 200X
DOI: 10.1039/b000000x

Incorporation of trace amounts of fluorophore-labelled proteins is used to study several optical properties and the growth history of protein crystals. Qualitative characterisations of the crystals have been performed by means of confocal laser scanning microscopy and polarisation microscopy. Our results first of all show that labelled proteins do not always act as micro-heterogeneous impurities for the crystals of their parent proteins and may behave differently towards different polymorphs of these protein crystals. Furthermore, labelled proteins may also show a distribution profile very different from their unlabelled counterparts when added as a heterogeneous impurity during crystallization. Nevertheless, a labelled protein that is incorporated in the growing crystals of its unlabelled counterpart can already provide valuable qualitative information on crystal symmetry and growth history, based upon its orientation, distribution and incorporation efficiency into the host crystals.

1 Introduction

Fluorescence is one of the most powerful physical phenomena used for studying macromolecules and their interactions in solution. Fluorescence has been used as a tool to study crystal growth[1]. Most proteins contain intrinsically fluorescent amino acids (mainly tryptophan), but at the high concentrations in a crystal this intrinsic fluorescence suffers from intra- and intermolecular quenching and is therefore not suitable to monitor crystal characteristics[2]. Instead, a small fraction of the macromolecules can be covalently labelled with a small fluorophore[3].

With respect to protein crystallisation, fluorophores have been used for two purposes. The first one is identifying protein crystals in high-throughput assays, e.g., for structural genomic projects[4,5]. For this, covalent labelling is not essential and fluorophores can be directly added to the crystallisation solution. In this case, small fluorophores, such as fluorescein molecules, can freely enter the aqueous compartments in the protein crystals and possibly interact with the proteins[6]. This is suitable for differentiating protein from salt crystals, since such dyes cannot enter or strongly interact with salt crystals. The second purpose is to study impurity distribution profiles during the crystallisation of macromolecules[3,4,7–14]. For these studies, fluorophores need to be covalently bound to the target macromolecule and the labelled macromolecules should incorporate into the growing crystal. Therefore, the molecules should be labelled at sites that do not block vital intermolecular contacts which markedly affect crystal packing or cause early cessation of crystal growth[15,16].

Labelling proteins is essentially a modification process in which the native macromolecule encounters a slight change in its molecular weight, molecular charge and contact points on the macromolecular surface. There is evidence that modifying or substituting residues on a macromolecule surface can lead to the formation of a low-entropy surface patch and thus enhance its crystallizability[17]. However, in most cases, these derivatised macromolecules act as micro-heterogeneous impurities which are preferentially incorporated at the early stages of nucleation and protein crystal growth[16].

Fluorophore-labelled tracer-proteins have mainly been used to study the physical chemistry of crystal growth. For instance, Matsui and co-workers modified the ε-amino group of the N-terminal lysine of hen egg white lysozyme (HEWL) with a fluorescent reagent, forming F-lysozyme, a modified macromolecule with extra 445 Daltons than the original molecular weight of HEWL (14.307 kD)[13]. They showed that at low concentration, F-lysozyme suppressed the nucleation and growth rate of the tetragonal polymorph of HEWL, while it did not affect the monoclinic form. This can be directly

† Electronic Supplementary Information (ESI) available: [Fig S1, the mathematical derivation of equation 1 and the hypothesis for F-BSA segregation from BSA crystals]. See DOI: 10.1039/b000000x/

[a] *Radboud University Nijmegen, Institute for Molecules and Materials, 6525 AJ Nijmegen, The Netherlands. Fax: 31 24 36 53393; Tel: 31 24 36 52558; E-mail: a.adawy@science.ru.nl*
[b] *Department of General Instrumentation, Faculty of Science, Radboud University Nijmegen, 6525 AJ Nijmegen, The Netherlands.*
[c] *Department of Biochemistry, Radboud Institute for Molecular Life Sciences, Radboud University Medical Center, 6525 GA Nijmegen, The Netherlands.*
‡ Permenant address: Physics Department, Faculty of Science, Ain Shams University, Cairo, Egypt.

explained by the location of the modified tail with respect to the intermolecular contact areas in the crystals. These modified tails are located within the contact areas of tetragonal HEWL crystals and outside these areas for the respective monoclinic polymorph. Such data corroborate those of Thomas and Chernov, who showed that modification of specific intermolecular contacts by acetylation, adversely affects the crystallisation processes[18]. Subsequently, Van Driessche and coworkers studied the effect of F-Lysozyme on the elementary growth steps on {110} faces of tetragonal HEWL crystals[19]. They reported that F-lysozyme molecules preferentially adsorb on steps, just like the native HEWL molecules, and are then incorporated into the crystal via the kinks on steps. They did not find any evidence for pinning of step advancement by F-lysozyme adsorbed at kinks. This was explained to be due to the very similar molecular surface and molecular weight of F-lysozyme compared to native HEWL.

In this report, we use fluorophore-labelled proteins (F-proteins) as tracers for studying protein crystal growth history. This is based upon the observation that F-proteins usually behave as micro-heterogeneous impurities for their native proteins, but can also be used as heterogeneous impurities for other macromolecules[8–10,13]. Thus, depending on their mode of interaction with the growing crystal, this should lead to different distribution efficiencies ranging from preferred incorporation to complete rejection. Furthermore, an F-protein may be non-uniformly incorporated during crystal growth if its segregation differs over the different growth sectors in a crystal. Consequently, the visible sector boundaries can provide information on the different growth rates of adjacent faces of this crystal.

We exploit a novel combination of optical microscopy in the transmission and polarisation mode and confocal fluorescence microscopy to extract growth and structural characteristics from four different protein crystals. In order to *in situ* monitor the crystal growth history, confocal fluorescence microscopy is used[20]. This allows to dissect a crystal into a finite number of transverse sections at different heights, which are afterwards reconstructed to give a 3D image. Optical properties of crystals depend on the assembly of the molecules within the crystals and the symmetry elements governing their spatial relations to one another. The preferential orientation of F-proteins within the crystals is monitored by polarisation microscopy, which can reveal crystallographic symmetry elements. Taking into account that many protein crystals do not exhibit the typical morphological features of regular crystals, such microscopic observations can be used as a tool for protein crystallographers in order to better characterize their crystals. In this study we focus our attention on the suitability of F-proteins of HEWL (F-Lyz), bovine insulin (F-ins) and bovine serum albumin (F-BSA) to characterize growth and properties of HEWL, insulin and bovine serum albumin (BSA) crystals. Here, we monitor the incorporation efficiency, distribution and orientation of F-proteins in the different protein host crystals for qualitative purposes. A quantitative study on impurity segregation will be presented elsewhere[21].

2 Experimental details

2.1 Materials

Hen egg-white lysozyme (Cat. No. L6876), fatty acid -free BSA (Fraction V, Cat. No. 85040C) and bovine insulin (lot # 069k09822) were purchased from Sigma-Aldrich and used without further purification. All other chemicals were of reagent grade.

2.2 Protein-labelling with fluorophores

For the preparation of the F-proteins 1 mg of the fluorescent dye DY-632-01 NHS ester ($C_{14}H_{49}N_3O_{14}S_3Na_2$; MW = 950.03 g/mol, Dyomics) was dissolved in 80 μl DMF (10.5 mM concentration), before being mixed with the different protein solutions. For HEWL there are seven possible sites for labelling with the activated DY-632-01: one α-amino group of the N-terminus and the ε-amino groups of the six lysine residues. HEWL was dissolved in 50 mM $NaHCO_3$ solution (pH 8.3 at 5 mg/ml concentration) before being mixed with fluorophores at a molar ratio of 1:1 and incubated in the dark for 2 hrs at 20^{o}C. After labelling, excess reagent was removed by gel filtration on a Sephadex G-25M column (GE-Healthcare) equilibrated in 100mM PBS-buffer (pH 7.4). The labelled fractions were afterwards eluted in dark centrifuge micro-tubes. Using basically the same protocol, about 2 of the 12 free N-termini of both the A- and B-chains of hexameric bovine insulin were labelled, with the molar ratio of the dye to insulin monomer set at 0.3. BSA has three lysine residues (Lys473, Lys349 and Lys116) which participate in binding fatty acids and two other lysine residues (Lys475 and Lys351) located on the molecular surface[22]. It was labeled in the same way with the dye at a 1:1 molar ratio. The absorbance of the eluted fractions was measured using a spectrophotometer (Lambda 35-UV/VIS, PerkinElmer instruments) after suitable dilution. HEWL, bovine insulin, BSA and DY-632-01 have absorbance bands peaking at 281 nm (ε: 2.64 $mg^{-1}.cm^{-1}$), 276nm (ε: 1.04 $mg^{-1}.cm^{-1}$), 279nm (ε: 0.65 $mg^{-1}.cm^{-1}$) and 631nm(ε :210.5 $mg^{-1}.cm^{-1}$), respectively. The fractions that showed the highest label content were combined. MALDI-TOF measurements of the selected fractions showed labelling efficiency of $>$50% for F-Lyz, and $>$90% for F-BSA and F-Ins.

2.3 Crystallisation

All crystallisation experiments were accomplished using the batch method. Tetragonal and monoclinic HEWL crystals were grown from solutions containing 4% w/v NaCl and 2% w/v $NaNO_3$ as precipitants mixed with 12 mg/ml and 10 mg/ml HEWL, respectively, dissolved in 0.1 M sodium acetate buffer (pH 4.5) at 20^oC[23]. Bovine insulin crystals were grown at 20^oC using the protocol described elsewhere[24], except that the final concentration of insulin was 0.75 mg/ml, and no acetone was used (pH 6.1) . BSA crystals were grown according to the protocol reported earlier for human serum albumin at a protein concentration of 100 mg/ml and 40% PEG 400 as precipitant in 0.1 M KH_2PO_4, pH 7 at 4^oC[22]. F-proteins were added into the various crystallisation solutions to a final concentration of 1% w/w of the unlabelled protein. The resultant solutions were then sandwiched between two glass cover slips separated by a rubber ring of 3 mm thickness in order to allow for both crystal growth and microscopic inspection.

2.4 Characterisation

A polarisation microscope (Leica DM-RX) was used in the transmission mode. Images were collected with a video camera (Evolution VF) and processed by means of Image Pro plus 2 software. The orientation dependent dichroism of the crystals was examined by the same microscope, using a single polariser. *In situ* observation of the preferential distribution of F-proteins into the different crystals was done on a Leica Confocal Laser Scanning Microscope (CLSM), using a HeNe laser (632.8 nm) as excitation source. The observation (fluorescence) wavelength range was 645 - 750 nm, using an excitation intensity of 17 % and a pinhole diaphragm diameter around 80 μm. The photomultiplier tube (PMT) gain was varied for different crystallisation groups from 250V to 570V, while all other settings were kept constant. In this way optimum image contrast is obtained and saturation of the confocal micrographs is avoided. Higher PMT voltages indicate lower fluorescence intensities, and thus lower incorporation levels, in the grown crystals (Table 1).

Table 1 The PMT voltages used for the different crystallisation combinations during CLSM examinations

Combination	PMT (V)
Monoclinic HEWL + F-Lyz	250
Tetragonal HEWL + F-Lyz	278
Rhombohedral insulin + F-Ins	500
Monoclinic BSA + F-BSA	570
Monoclinic HEWL + F-Ins	385
Tetragonal HEWL + F-Ins	315
Tetragonal HEWL + F-BSA	412
Monoclinic HEWL + F-BSA	424

3 Results and discussion

In principle, protein labelling introduces slight modifications and subsequently micro-heterogeneity into the native protein macromolecules[18]. According to the established theories, these F-proteins should act as micro-heterogeneous impurities for their respective native protein crystals and thus are expected to be incorporated strongly at the early stages of crystal growth[16,25,26]. This should facilitate monitoring the history of crystal growth. Moreover, adding the labelled version of a protein into the crystallisation solution of another protein should reveal the behaviour of a heterogeneous impurity during the crystallisation of the protein under investigation. In order to study both conditions we used different F-protein # protein combinations as shown below. We have found a significant diversity which seems related to the crystal form, but more probably to the investigated F-protein # protein combinations.

3.1 Tetragonal HEWL

3.1.1 F-Lyz into tetragonal HEWL crystals. The results of this combination corroborate earlier theoretical and experimental studies. Therefore, we will present this as our model system to also outline the novel setups and characteristics one can extract from microscopic inspection.

Crystal morphology and optical absorption. When grown in the presence of F-Lyz, the crystals show a bluish colour under a bright field microscope, which is a consequence of the strong absorbance band of the incorporated fluorophore in the red-infrared part (620 - 750 nm) of the visible spectrum (Fig. 1).

Tetragonal HEWL crystals grow through two main crystallographic facets; $\{110\}$ and $\{101\}$. The final morphology of the crystals depends on the level of supersaturation as shown earlier[27,28]. At low supersaturation, $\{101\}$ grow faster than $\{110\}$ and the crystals become oblong along $\langle 001\rangle$. At extremely high growth rates, $\{110\}$ grow much more rapidly than $\{101\}$ and the crystals tend to become flattened bipyramids with edges pointing towards $\langle 100\rangle$. This leads to differently shaped $\{110\}$ and $\{101\}$ growth sectors in the crystals (Fig. 2). The optical transmission micrographs reveal a difference in the colour for the two kinds of growth sectors, $\{110\}$ being more bluish/greenish than $\{101\}$ (Fig. 3 a). This difference indicates that F-Lyz is preferentially incorporated in the $\{110\}$ sectors.

Dichroism. When the crystals are monitored along $\langle 110\rangle$ using a single polariser, the fluorescent dye shows dichroism, while they do not show this effect along $\langle 001\rangle$. Fig. 3 demonstrates that the crystals show a clear blue colour, i.e., red light is absorbed, when viewed along $\langle 110\rangle$ with the polariser parallel to $[1\bar{1}0]$, but are only very pale blue with the polariser parallel to [001]. The preferential occurrence in the $\{110\}$

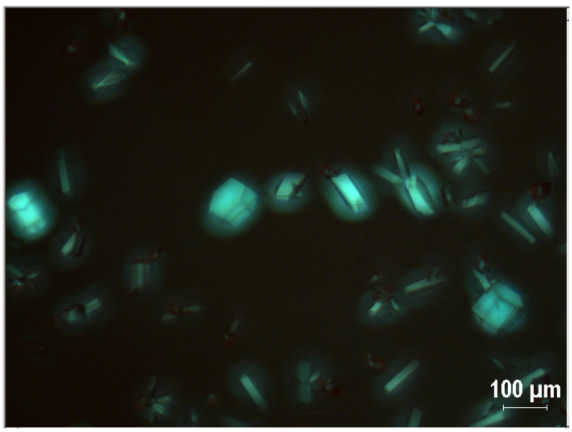

Fig. 1 Polarisation micrograph of tetragonal HEWL crystals grown in the presence of 1% (w/w) F-Lyz in their mother liquor. Here the crystals are imaged between crossed polarisers to eliminate the bluish background colour of the mother liquor.

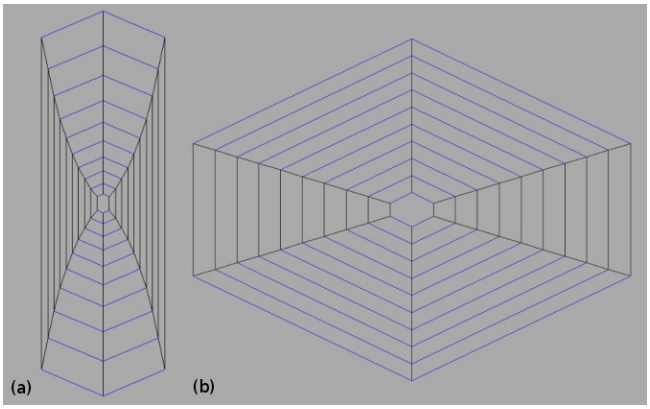

Fig. 2 $(1\bar{1}0)$ cross-section profiles showing the $\{110\}$ and $\{101\}$ growth sectors of tetragonal HEWL, calculated in SHAPE suite. The growth morphology is determined by two crystallographic faces: $\{101\}$ (blue) and $\{110\}$ (grey). If the growth rate of $\{101\}$ prevails, the resultant crystal is oblong along $\langle 001 \rangle$ (a). If the growth rate of $\{110\}$ prevails, the crystals tend to be extended along $\langle 110 \rangle$ (b).

sectors and the dichroic effect indicate that the fluorophores have a preferential position and orientation in the crystals and, therefore, they are not randomly distributed. To our knowledge, this effect was not reported before for protein crystals, while it can aid in determining the crystal symmetry.

The observed dichroism of the F-Lyz doped tetragonal HEWL crystals complies with their 422 point group symmetry. Viewed along the $\langle 001 \rangle$ 4-fold axis, no change in colour is observed upon rotation of the polariser over 90^o. On the other hand, when viewed along a $\langle 110 \rangle$ 2-fold axis a 90^o rotation gives a change in colour, but a rotation over 180^o yields no change. This dichroism also indicates a preferential orientation of the dye attached to the labelled macromolecules in the HEWL crystal lattice. If the E-vector of the polarised light beam is parallel to the plane of conjugated π-bonds of the fluorophore, the red component of the beam is absorbed, giving a bluish colouration of the crystals (Fig. 3). Since this bluish colouring was observed for all polarisation (E-vector) directions when the crystal was viewed along $\langle 001 \rangle$ (Fig. 3 c,d), as well as for the polarisation direction parallel to [110] when viewed along $[1\bar{1}0]$ (Fig. 3 a), it follows that the conjugated plane of the fluorophore is oriented preferentially parallel to $\{001\}$ in the crystal. If the E-vector is parallel to [001], i.e. perpendicular to the conjugated π-bond plane, little absorption occurs and the crystal is only coloured palely (Fig. 3 b).

*Photo-bleaching.*It can be used to independently confirm that the fluorophores are bound to protein molecules and that they cannot diffuse freely within the crystals. This is done by exposing a part of a crystal using a highly intense laser beam and re-examining its fluorescence distribution afterwards. This is illustrated in Fig. 4 and confirms that the F-Lyz is rigidly incorporated in the crystalline lattice, being covalently bonded to HEWL, and not freely diffusing within the aqueous compartments in the crystal*.

*Structural biology confirms the dichroic observations.*In order to understand the preferential orientation of fluorophores, we have to look into the native HEWL molecule, which is ellipsoidal and has 6 lysine residues on its surface: Lys 1 and Lys 116 along the z-axis, and Lys 33 and Lys 97 along the y-axis so that these four are almost equally distributed on the molecule surface. Lys 96 and Lys 13 are located close to Lys 97 on the same side along the x-axis (Fig. 5). Of all lysine residues, Lys 97 and Lys 33 were shown earlier to have the highest reactivity for labelling[29]. Taking into account the initial ratio of the dye to protein during the labelling experiments (1:1) and the labelling efficiency of about 50%, we expect that the labelled residues are those lying along the y-axis and therefore the fluorophore is expected to be covalently bonded to Lys 97 or Lys 33 in such a way that the conjugated π-bonds of the fluorophores (Fig. 6) lie in the x-z plane of the molecule. The latter plane is almost normal to the crystallographic c-axis (and thus $\langle 001 \rangle$) of the tetragonal crystal †.

*Spatial distribution of F-proteins (micro-heterogeneous impurities).*CLSM images displayed in Fig. 7(a) show that crystals monitored along their c-axis, i.e., $\langle 001 \rangle$), yield stronger fluorescence than those monitored along $\langle 110 \rangle$. This is a logical consequence of the fact that these micrographs are obtained by using non-polarised laser light. For the crystals viewed along $\langle 110 \rangle$, only laser polarisation directions near

∗ A similar experiment for a monoclinic HEWL crystal was also performed over 24 hrs and diffusion also was observed (Fig S1)

† look at http://www.rcsb.org/pdb/explore/jmol.do?structureId=2YVB& opt=3

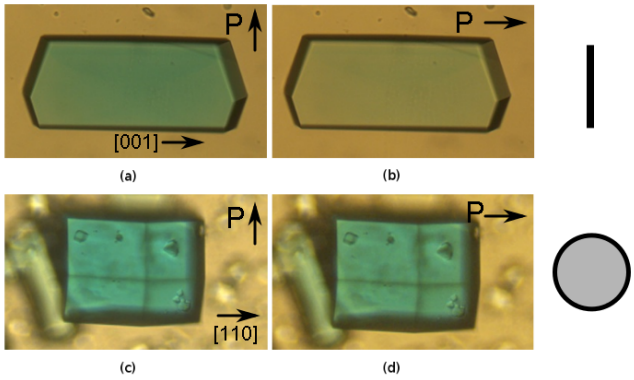

Fig. 3 Tetragonal HEWL crystal, grown in the presence of 1% (w/w) F-Lyz, viewed under the polarisation microscope along [110] (a,b) and along [001] (c,d) using a single polariser. Rotating the polariser 90^o (from a to b, and c to d) shows that the crystal exhibit dichroism only when viewed along [110]. On the right, the plane of conjugated π-bonds in both cases is shown.

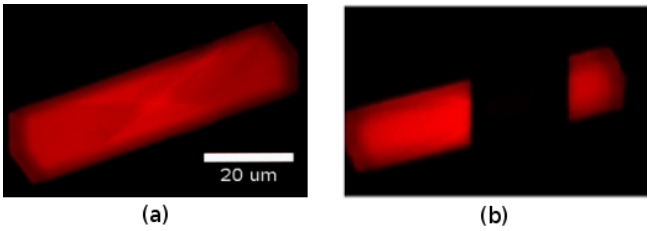

Fig. 4 CLSM micrographs of the central {110} slice of a tetragonal HEWL crystal (a). The highest fluorescence intensity is located at the central core of the crystal. At 2 hrs after photo-bleaching a section of this crystal no diffusion of fluorophores was detected (b), confirming that the dye is only bound to protein molecules and not freely moving within the crystal.

[1$\bar{1}$0] lead to absorption and thus fluorescence, whereas all polarisation directions contribute to the light absorption and subsequent fluorescence for the crystals viewed along ⟨001⟩. Viewing the crystals along their ⟨110⟩ direction shows that the distribution of F-Lyz is not homogeneous throughout the crystals, but differs for the two main crystallographic faces, with a higher incorporation within the {110} growth sectors as compared to the {101} sectors (Fig. 7 (b). In addition, the crystal cores have the highest fluorescence intensity which decreases towards their peripheries. This confirms that F-Lyz acts as a structurally related, i.e., micro-heterogeneous impurity for HEWL that is preferentially incorporated at the early stages of crystal growth[26]. This leads to a substantial depletion of F-Lyz in the crystallisation solution during further growth.

*Crystal growth rate and history.*In Fig.7 (c), the sector boundaries, which are formed between the prismatic {110} and pyramidal {101} faces, are curved in a way revealing that

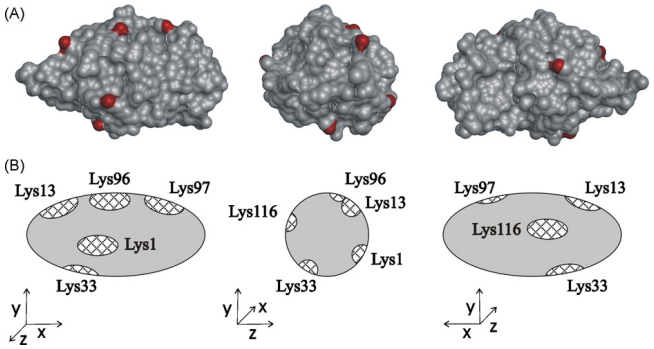

Fig. 5 The ellipsoidal HEWL molecule with 6 lysine residues (a); A schematic drawing showing the molecules rotated around the y-axis in 90^o steps (b). Adapted from[29] with the kind permission of the authors & publisher (License # 3240681117906)

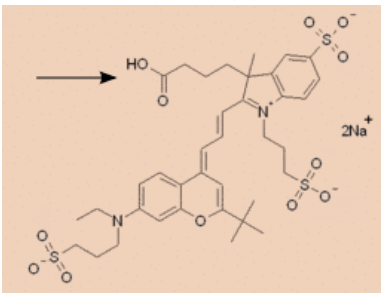

Fig. 6 The chemical structure of DY-632. The arrow points to the carboxyl group that is activated as the NHS-ester.

the {101} faces continued to grow for a longer time or at a higher rate than the {110} faces. This effect is a function of the initial supersaturation and is clearly visualised in the presence of F-proteins, but is also very weakly visible in uncontaminated crystals (Fig. 8). In the latter case, the optical image contrast of the sector boundaries points to a slightly different refractive index of the adjacent sectors, which is likely due to a slightly different composition (e.g. water, NaCl, impurity content) of these regions, which may retard the growth of certain faces and change the final shape of the crystal.

The slope angle of the sector boundaries, φ = atan(dy/dz), is related to the relative growth rates of the adjacent {101} and {110} faces according to equation (1), the derivation of which is given in the supplementary information†.

$$\frac{R_{101}}{R_{110}} = 0.3056 + \sqrt{\frac{0.8133}{sin^2\varphi} - 0.8133} \qquad (1)$$

These data were calculated for the crystal and have allowed for mapping the growth history of the crystal. From the corresponding measurement of the sector boundary slope of the crystal shown in Fig. 9 the relative growth rates of the {110} and {101} faces as a function of the position in the crystal,

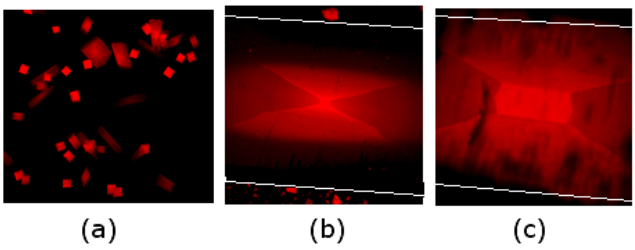

Fig. 7 CLSM micrograph of tetragonal HEWL crystals grown in the presence of 1% (w/w)F-Lyz: (a) shows the difference in fluorescence intensity for crystals viewed along ⟨001⟩ (high) and ⟨110⟩ (low); (b) Along ⟨110⟩, the non-uniform distribution of F-Lyz is shown at the central plane of the crystal ; (c) At a slightly higher plane, the central upward {110} growth sector are more clearly visible.(White lines are drawn to show the boundaries of the crystal.)

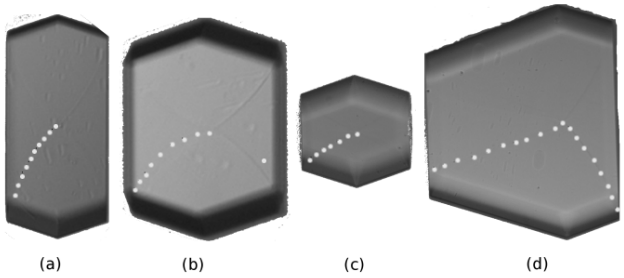

Fig. 8 Transmission micrographs showing {110}/{101} sector boundaries in tetragonal HEWL crystals grown at low (a), moderate (b), and high (c) initial supersaturation. The presence of impurities can also affect the crystal morphology if symmetric facets do not grow equally fast because of surface blockage or the presence of different densities of screw dislocations (d). All crystals are displayed at the same magnification.

starting from the central nucleus. It can be seen that at the early stage of growth R_{110}/R_{101} is about 0.5, which is characteristic for high supersaturation[27,28]. Upon further growth the supersaturation decreases by depletion of the solution, leading to a decrease in $R_{(110)}/R_{(101)}$. Finally, the {101} still able to grow, but the {110} face is completely blocked. Probably the 110 face enters the so-called dead zone where growth is inhibited by impurity (F-Lyz) adsorption[30]. Thus, the crystal growth becomes dominated by one type of growth sector, {101}. This agrees with the lower uptake of F-Lyz into these {101} facets.

*Fossil patterns.*Using F-proteins as tracers, CLSM can reveal the different growth sectors as well as fossil patterns of spiral hillocks or 2D islands on the crystal surface. Here, we show an example of this novel application: 2D islands in {110} sectors exhibiting an elongated lens-shaped morphology with tips pointing towards ⟨110⟩ (Fig. 10). The same pattern, amongst others, have been earlier observed *in situ* by high-resolution phase contrast optical microscopy on the {110} faces of growing HEWL crystals[31]. This is the first time these patterns are monitored by CLSM and they demonstrate that different step orientations during crystal growth also lead to local differences in impurity uptake.

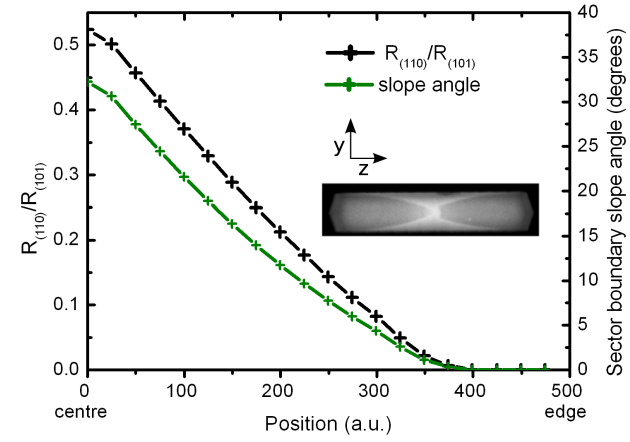

Fig. 9 Sector boundary slope angle between the growth sectors of the adjacent {101} and {110} as a function of the distance from the crystal core. This is directly related to the relative growth rates of the {101} to {110} faces at different stages, which reflects the history of crystal growth.

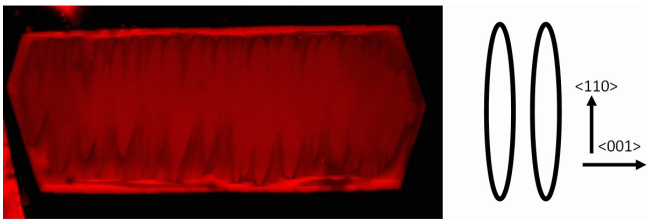

Fig. 10 (left) Fossil pattern of spiral or 2D island growth in a {110} sector of tetragonal HEWL crystal monitored by CLSM; (right) Shape and orientation of the spiral patterns as reported in the literature[31,32].

3.1.2 F-Ins and F-BSA into tetragonal HEWL. These combinations are illustrative for the effects of heterogeneous impurities (bovine insulin and BSA) on crystal growth. Earlier, we touched upon the effects of the unlabelled impurities on the morphology of tetragonal HEWL[33]. Assuming that their fluorescent derivatives will show a similar behaviour as an impurity, we can monitor their spatial distribution within the crystals.

We observed that the presence of F-Ins in the crystallisation solution adversely affects the nucleation of tetragonal HEWL

crystals. The crystals grow only as oblong crystals which indicates that F-ins did not affect the supersaturation level. As expected for a heterogeneous impurity, the cores of these crystals showed no fluorescence (Fig. 11a). In contrast to F-Lyz, F-Ins becomes preferentially distributed, and thus completely consumed, into the $\{101\}$ sectors, rendering the edges of the crystals F-ins-free.

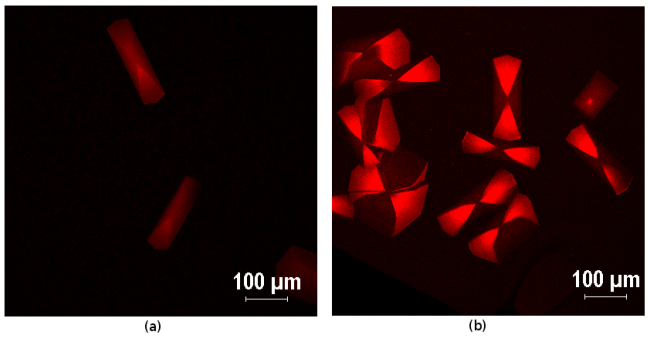

Fig. 11 CLSM micrographs at the central (110) plane of tetragonal HEWL crystals grown in the presence of 1% (w/w) F-ins (a) and F-BSA (b) in their mother liquor.

F-BSA mimics the action of F-ins on the nucleation and the impurity-free crystals core, but oblong as well as symmetric tetragonal crystals are observed. Moreover, its incorporation leads to the development of cracks in some of the symmetric crystals in both crystallographic sectors. Surprisingly, F-BSA is completely rejected from the $\{110\}$ faces and is preferentially trapped by the $\{101\}$ faces (Fig. 11b). This result is completely inconsistent with what is observed for unlabelled BSA as a contaminant, which is thoroughly investigated elsewhere[21]. This again demonstrates that labelled proteins may significantly deviate in behaviour from their unlabelled counterparts, but still the obtained data can provide valuable information on crystal history and impurity-crystal interaction.

3.2 Monoclinic HEWL

Monoclinic HEWL crystals resemble the tetragonal polymorph in their preferential trapping of F-Lyz, but differ in their reaction towards the other F-proteins.

*Crystal morphology and optical absorption.*Under the applied crystallisation conditions, the monoclinic HEWL crystals grow as oblong crystals along [010], bounded by the crystallographic habit faces (010), $(0\bar{1}0)$, $(10\bar{1})$, (101) and $\{001\}$. The planar (010) face has the highest growth rate. The opposite face $(0\bar{1}0)$ is not related to (010) by symmetry, and is largely blocked. This polar growth of the crystal point group 2 was reported previously[34,35]. The $\{001\}$ faces have usually a very high growth rate and are consequently hidden by slowly growing $(10\bar{1}$ and (101) facets, which cover the largest surface area on the crystals (Fig. 12).

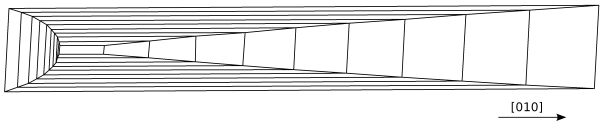

Fig. 12 Calculated growth profile for a monoclinic crystal using the SHAPE suite, showing polar growth in the [010] direction.

The optical transmission micrographs show that F-Lyz is readily incorporated into monoclinic HEWL crystals. Interestingly, the crystals have the same size and shape with or without F-Lyz, which indicates that F-Lyz hardly affects the crystal growth and habit. Unlike the mother liquor of tetragonal crystals, here the crystallisation solution was colourless afterwards, while the crystals where very bluish/greenish and the intensity of colouration is almost uniform throughout the crystals (Fig. 13). This indicates that F-Lyz was equally incorporated as HEWL in the crystals, which may point to a unity segregation coefficient. In addition, this can be attributed to the difference between the precipitating anions used to grow monoclinic (NO_3^-) and tetragonal (Cl^-) HEWL crystals. NO_3^- was shown earlier to result in lower solubility, and subsequently higher supersaturation and driving force for crystallisation, compared to Cl^-[36].

*Dichroism.*Viewing the crystals along their $(10\bar{1})$ plane, they show dichroism upon 90^o rotation with one fixed polariser (Fig. 14). The crystal colour fades away when the crystallographic b-axis moves parallel to the polarisation direction. Similar to tetragonal HEWL crystals, this confirms that there is a preferential orientation of the fluorophore conjugated π-planes in the crystals.

*Spatial distribution of different F-proteins.*The confocal micrographs show that the fluorescence intensity of the monoclinic crystals is much higher than that of the tetragonal crystals grown at the same molar ratio of native to labelled HEWL, and analysed at about the same CLSM setting. In contrast to the tetragonal crystals as well the fluorescence is almost homogeneously distributed over the crystals except for a slightly higher value for the rounded $(0\bar{1}0)$ faces (Fig. 15a).

While monoclinic HEWL crystals show a high tolerance for F-Lyz incorporation within their sectors, they very strongly reject incorporation of F-Ins (Fig. 15b) and nearly completely that of F-BSA (Fig. 15c). The luminescence intensity of the crystals is equal to or less than the very weak background luminescence resulting from labelled proteins

in solution or light scattering, which can only be detected using the highest PMT voltages (Table 1). This shows that

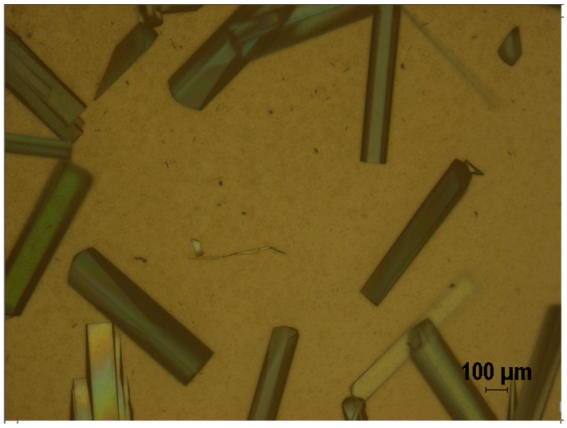

Fig. 13 Overview of monoclinic HEWL crystals grown in the presence of F-Lyz in their mother liquor. The crystals trapped all the F-lyz, leaving the depleted solution almost colourless.

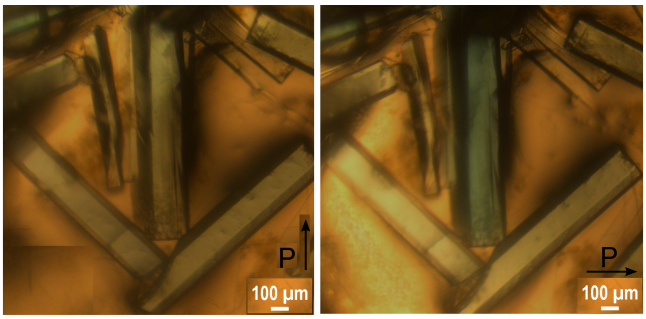

Fig. 14 Polarisation micrographs of a F-lyz containing monoclinic HEWL crystal which encounters dichroism upon 90^o rotation (a to b). A single polariser is used; its direction is indicated by an arrow.

when a certain macromolecule crystallizes in different polymorphic forms, every polymorph reacts very differently toward impurities with respect to the incorporation level and pattern. Hence, we here present sound evidence from the perspective of impurity incorporation that it is a good practice to test several polymorphs of a protein, if available, in crystallisation trials. A mechanistic discussion of this interesting observation is beyond the scope of this report and will be presented elsewhere[21].

3.3 Rhombohedral Bovine Insulin

The bovine insulin monomer consists of two polypeptide chains (A and B) linked by disulphide bonds, which normally associate with another monomer to form dimers. During crystallisation, three dimers assemble together into a cylindrical hexamer, which makes up the asymmetric unit of the unit cell. The crystals then grow in a rhombohedral lattice (Fig. 16)

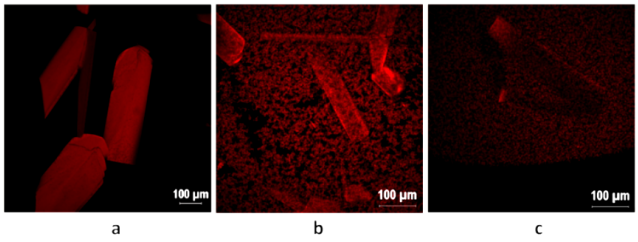

Fig. 15 CLSM micrographs of the central slices in monoclinic HEWL crystals grown in the presence of F-Lyz (a), F-Ins (b) and F-BSA (c) in their crystallisation solutions.

with space group R3, in which the asymmetric units are arranged at the corners of the unit cell with a tilt of 258^o out of the {100} crystallographic planes. The growth of this crystal occurs through 2D nucleation and spiral growth on {100}, resulting in a rhombohedral morphology bounded by {100} faces[37].

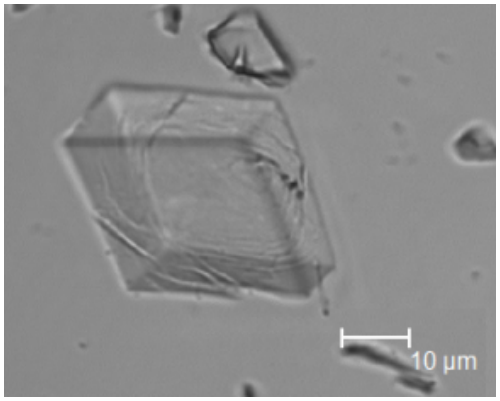

Fig. 16 Bright field transmission micrograph of a reference rhombohedral bovine insulin crystal bounded by {100} faces.

*Spatial distribution of F-ins.*According to the established theory, one would expect that F-ins should behave as a micro-heterogeneous impurity for native insulin, which would be incorporated mostly at the early stages of crystal growth. In contrast, CLSM showed that the crystals did not possess fluorescent cores and the incorporation of F-Ins is only observed towards the peripheries of the crystals (Fig. 17). This indicates that F-ins acts here as a heterogeneous impurity.

*Structural biology explains the unexpected behaviour of F-ins in insulin crystals.*The complete segregation of F-ins except for crystal peripheries can again be explained by looking into the molecular surface and its environment. From the molecular structure, B chains have lysine residues which are involved in intermolecular contacts. In addition, both A and B chains have a free N-terminus, which lies at the surface of

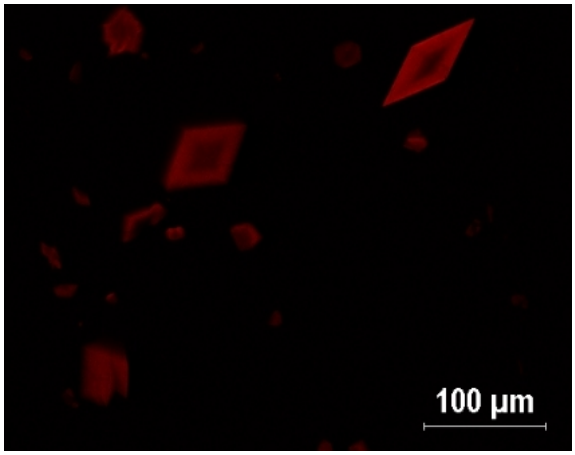

Fig. 17 CLSM micrographs of rhombohedral bovine insulin crystals grown in the presence of 1% (w/w) F-Ins in their mother liquor.The micrographs display the central plane within the crystals.

the hexamer, and is thus available for labelling. Earlier, Bergeron and co-workers showed that the significant release of water molecules upon the attachment of an insulin molecule to a growth site may reflect the hydrophobic nature of some intermolecular interactions in insulin crystals[38]. Hence, labelling up to two of the potential 12 N-terminal amino groups in a hexamer with a hydrophilic fluorophore is expected to seriously perturb the crystal packing as well as the crystal growth. Therefore, F-ins, despite its very close structural relationship to insulin monomers, acts as an impurity which is initially rejected by the bovine insulin crystal. This explains its incorporation only at the later stages of crystal growth, which is the usual behavior of a heterogeneous impurity[26].

*No dichroism, but birefringence.*Using a single polariser in the polarisation microscope, no dichroism was observed for the insulin crystals. The absence of this phenomenon here may be related to the fact that F-ins is initially expelled from the crystals and upon incorporation at later stage eventually blocks further growth. However, under a polarisation microscope with two crossed polarisers, the crystals showed an unusual sort of birefringence. The crystals changed colour from bright bluish to dark upon 60^o rotation and restored their bright colour by a further 30^o rotation in the same direction. This unusual $60^o/30^o$ birefringence might be due the presence of two preferential orientations of the fluorophores in the insulin hexamer. Molecular modelling may be tried to confirm this hypothesis, but this is beyond the scope of this article.

3.4 BSA crystals

*Crystal morphology and optical absorption.*The BSA crystals are very fragile, small, and transparent and display an elongated lozenge shape (Fig. 18). In a number of cases cross twins could be identified. The morphology of most crystals seems to comply -on average- with point group 2/m (monoclinic), which was also recently reported elsewhere[39,40], though we used a very different crystallisation protocol.

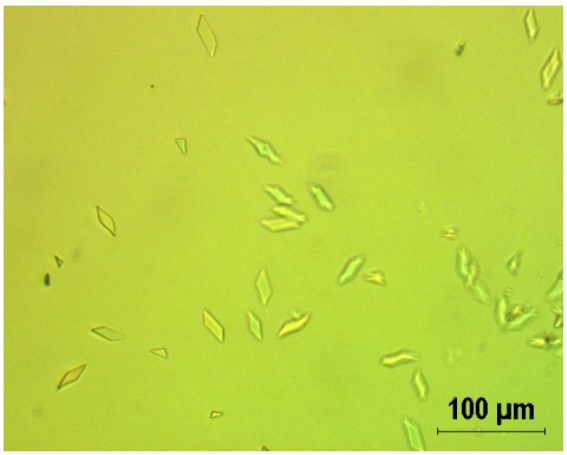

Fig. 18 Polarisation micrograph of BSA crystals grown in the absence of fluorophores, the crystals had no detectable birefringence.

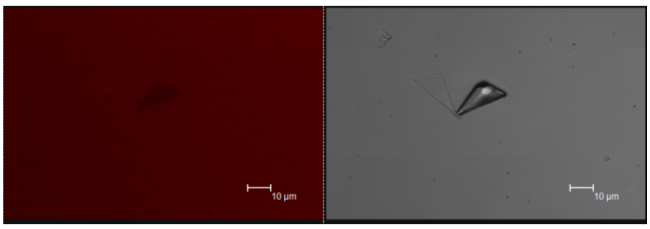

Fig. 19 CLSM micrograph (left panel) and its bright field transmission counterpart (right panel) of BSA crystals grown in the presence of 0.5% F-BSA in their mother liquor. The very weak background light intensity results from luminescence of F-BSA in the solution and from light scattering.

*Spatial distribution of F-BSA.*The presence of F-BSA does not change the nucleation and growth properties of BSA crystals. CLSM did not detect any fluorescence in the crystals, not even at their peripheries. This indicates that either F-BSA was completely rejected from the BSA crystal lattice (Fig. 19) or was incorporated to such an extent that its fluorescence was largely lost by quenching. The latter probability is less likely, because we screened the crystals with very low up to high PMT voltages (Table 1), yet we only observed fluorescence from the surrounding solution.

Neither dichroism nor birefringence(between crossed polarisers) is observed for this combination, regardless of crystal

orientation. The absence of the former phenomenon is probably due to the complete segregation of F-BSA from the BSA crystals, as is the case for insulin crystals. Presumably, the crystals were too small to show birefringence.

We propose that the apparently complete segregation of F-BSA from the BSA crystals is due to the presence of the highly charged fluorophore at a critical intermolecular contact point in the protein , such that it blocks incorporation of the labelled protein in the growing crystal by sterical and/or charge repulsion. A hypothetical explanation which still needs further confirmation is presented in the supplementary information†.

4 Conclusions

In this study, we demonstrate that several elementary (bio-)physical properties of protein crystals can be easily observed by adding trace amounts of fluorophore-labelled proteins to the mother liquor of the target protein. Routine qualitative inspection using polarisation and confocal fluorescence microscopy can reveal elements like crystal growth habit, history and symmetry as well as spatial distribution and orientation of impurities in the crystals. This is a powerful approach to visualize several aspects of the crystal growth process, without the need to record the entire experiment or using more sophisticated facilities, such as differential phase contrast and atomic force microscopy.

Our study also demonstrates that the incorporation and optical properties of the labelled proteins can vary strongly depending on the target protein and type of the labelled *impurity*. From the various investigated combinations, we conclude that F-proteins:

1. in case of preferential incorporation, act as tracers, which facilitates identification of protein crystals, but also provides rapid insight into the crystal growth history and symmetry.

2. in case of their segregation, can still define the crystal periphery and may contribute to unravelling the role of the various biophysical factors that can affect crystal growth (e.g., surface hydrophobicity, charge distribution, intermolecular interaction). In this context it should be useful to study different fluorophores and/or labelling protocols, since the corresponding F-proteins may show different incorporation profiles and hence provide complementary information.

3. as a heterogeneous impurity, may act very different from their unlabelled counterparts. Also in this context testing various labelling protocols may be very informative.

Our study also shows that the distribution of impurities is not usually uniform over the crystals and can vary for the different growth sectors, cores and peripheries of the crystals. This implies that the diffraction quality of the crystals is position dependent. Our evidence that a crystal contains sites with relatively higher perfection advocates the use of X-ray microbeams and rastering to scan the crystals for such sites, which as yet can can only be applied in a small number of beamlines. In principle, using fluorophore-labelled protein should also allow to pre-identify these sites.

Summarizing, studying the optical properties of protein crystals *illuminated* with F-proteins can provide highly relevant information on their growth and perfection, and contribute to improving crystal quality and structural resolution. This can reveal more about the macromolecular structures of those proteins that are still not solved to high degrees of precision.

5 Acknowledgement

We thank Petra Bovee-Geurts, Department of Biochemistry, Radboud Institute for Molecular Life Sciences, Radboud University Medical Center, for technical support in the fluorescent labelling of HEWL. This research was funded by The Netherlands Foundation for Scientific Research through its Chemical Council (NWO-CW, project 700.57.022).

References

1 W. Van Enckevort and E. Visser, *Philosophical Magazine B*, 1990, **62**, 597–614.
2 J. R. Lakowicz and B. R. Masters, *Principles of fluorescence spectroscopy*, Springer, 3rd edn, 2008.
3 R. Chen, *Biochemical and Biophysical Research Communications*, 1970, **40**, 1117–1124.
4 E. Forsythe, A. Achari and M. L. Pusey, *Acta Crystallographica Section D*, 2006, **62**, 339–346.
5 M. L. Pusey, *Crystal Growth Design*, 2011, **11**, 1135–1142.
6 A. Cvetkovic, A. Straathof, D. Hanlon, S. Van der Zwaag, R. Krishna and L. Van der Wielen, *Biotechnology and Bioengineering*, 2004, **86**, 389–398.
7 K. Kurihara, S. Miyashita, G. Sazaki, T. Nakada, S. Durbin, H. Komatsu, T. Ohba and K. Ohki, *Journal of crystal growth*, 1999, **196**, 285–290.
8 C. Caylor, I. Dobrianov, C. Kimmer and R. Throne, *Physical review E*, 1999, **59**, 3831–3834.
9 C. L. Caylor, I. Dobrianov, S. G. Lemay, C. Kimmer, S. Kriminski, K. D. Finkelstein, W. Zipfel, W. W. Webb, B. R. Thomas, A. A. Chernov and R. E. Thorne, *Proteins-Structure Function and Genetics*, 1999, **36**, 270–281.
10 Y. Iimura, I. Yoshizaki, H. Nakamura, S. Yoda and H. Komatsu, *Jpn. J. Appl. Phys.*, 2003, **42**, 5831–5836.
11 Y. Iimura, I. Yoshizaki, S. Yoda and H. Komatsu, *Crystal Growth Design*, 2004, **5**, 295–300.
12 Y. Iimura, I. Yoshizaki, H. Nakamura, S. Yoda and H. Komatsu, *Crystal Growth Design*, 2004, **5**, 301–305.
13 T. Matsui, G. Sazaki, H. Hondoh, Y. Matsuura, T. Nakada and K. Nakajima, *Journal of Crystal growth*, 2006, **293**, 415–422.
14 A. Van Driessche, G. Sazaki, F. Otalora, F. Gonzalez-Rico, P. Dold, K. Tsukamoto and K. Nakajima, *Crystal Growth Design*, 2007, **7**, 1980–1987.

15 J. Sumida, E. Forsythe and M. Pusey, *Journal of Crystal Growth*, 2001, **232**, 308–316.

16 A. Chernov, *Journal of structural biology*, 2003, **142**, 3–21.

17 Z. Derewenda, *Structure*, 2004, **12**, 529–535.

18 B. Thomas and A. Chernov, *Journal of crystal growth*, 2001, **232**, 237–243.

19 A. Van Driessche, G. Sazaki, G. Dai, F. Otalora, J. Gavira, T. Matsui, I. Yoshizaki, K. Tsukamoto and K. Nakajima, *Crystal Growth and Design*, 2009, **9**, 3062–3071.

20 S. Wright and G. Schatten, *Journal of electron microscopy techniques*, 1991, **18**, 2–10.

21 A. Adawy, E. van der Heijden, J. Hekelaar, W. De Grip, W. van Enckevort and E. Vlieg, to be submitted.

22 S. Sugio, A. Kashima, S. Mochizuki, M. Noda and K. Kobayashi, *Protein engineering*, 1999, **12**, 439–446.

23 A. Adawy, E. Rebuffet, S. Tornroth-Horsefield, de Grip WJ, W. van Enckevort and E. Vlieg, *Crystal Growth & Design*, 2013, **13**, 775–781.

24 I. Reviakine, D. Georgiou and P. Vekilov, *Journal of the American Chemical Society*, 2003, **125**, 11684–11693.

25 D. C. Carter, K. Lim, J. X. Ho, B. S. Wright, P. D. Twigg, T. Y. Miller, J. Chapman, K. Keeling, J. Ruble, P. G. Vekilov, B. R. Thomas, F. Rosenberger and A. A. Chernov, *Journal of Crystal Growth*, 1999, **196**, 623–637.

26 B. Thomas, A. Chernov, P. Vekilov and D. Carter, *Journal of Crystal Growth*, 2000, **211**, 149–156.

27 R. Grimbergen, E. Boek, H. Meekes and P. Bennema, *Journal of crystal growth*, 1999, **207**, 112–121.

28 S. Durbin and G. Feher, *Journal of Crystal Growth*, 1986, **76**, 583–592.

29 F. Dismer and J. Hubbuch, *Journal of Chromatography A*, 2007, **1149**, 312–320.

30 M. Plomp, A. McPherson and A. Malkin, *Proteins: Structure, Function, and Bioinformatics*, 2003, **50**, 486–495.

31 P. Dold, E. Ono, K. Tsukamoto and G. Sazaki, *Journal of Crystal Growth*, 2006, **293**, 102–109.

32 S. Durbin, W. Carlson and M. Saros, *Journal of Physics D: Applied Physics*, 1993, **26**, B128.

33 A. Adawy, K. Marks, W. de Grip, W. van Enckevort and E. Vlieg, *CrystEngComm*, 2013, **15**, 2275–2286.

34 M. Heijna, W. v. Enckevort and E. Vlieg, *Crystal Growth and Design*, 2007, **8**, 270–274.

35 H. Hondoh, G. Sazaki, S. Miyashita, S. Durbin, K. Nakajima and Y. Matsuura, *Crystal Growth Design*, 2001, **1**, 327–332.

36 M. M. Ries-Kautt and A. F. Ducruix, *Journal of Biological Chemistry*, 1989, **264**, 745–748.

37 K. Waizumi, M. Plomp and W. van Enckevort, *Colloids and Surf. B: Biointerfaces*, 2003, **30**, 73–86.

38 L. Bergeron, L. Filobelo, O. Galkin and P. Vekilov, *Biophysical journal*, 2003, **85**, 3935–3942.

39 K. Majorek, P. Porebski, A. Dayal, M. Zimmerman, K. Jablonska, A. Stewart, M. Chruszcz and W. Minor, *Molecular Immunology*, 2012, **52**, 174–182.

40 A. Bujacz, *Acta Crystallographica Section D: Biological Crystallography*, 2012, **68**, 1278–1289.